Tectonics

Supporting Information for

Geometry and kinematics of the Grant Range brittle detachment system, eastern Nevada, U.S.A.: an end-member style of upper-crustal extension

Sean P. Long[1,2] and Jerome P. Walker[3]

[1]*Nevada Bureau of Mines and Geology, University of Nevada, Reno, NV 89557, U.S.A.*

[2]*Now at: School of the Environment, Washington State University, Pullman, WA 99164, U.S.A.*

[3]*Consulting geologist, Reno, NV 89509, U.S.A.*

Contents of this file

Introduction

Supporting information for this paper includes text, figures, and tables that give information on thicknesses of Grant Range rock units, supporting data for the $^{40}Ar/^{39}Ar$ date for sample GR63, supporting data for oil field well logs, data constraining the geometry of set 1 detachment faults, description of the techniques and data used to estimate tilting accompanying set 2 normal faulting, and detailed descriptions of the geometries and field relations of set 1 detachment faults.

Text S1. Thicknesses of Grant Range rock units

Thicknesses of stratigraphic units in the map area were estimated from the cross sections where possible. In many cases, particularly for Cambrian and Ordovician rock units, complete sections were not exposed, and only minimum thicknesses could be estimated. For several of these units, published thickness estimates from nearby studies in the Grant Range were used (Table S1). However, for several members of the Cambrian Sidehill Spring Formation and several formations of the Ordovician Pogonip Group, complete thicknesses are not exposed anywhere in the Grant Range. For these units, minimum tectonic thicknesses, as estimated from the cross sections, are shown (Table S1). Even using these minimum thicknesses, the

cumulative thickness of the Cambrian carbonate section above the Prospect Mountain Quartzite in the map area is 11,700 feet. This is thicker than, but comparable to, cumulative thickness estimates of 9,500-10,000 feet for these rocks in the southern Grant Range (Cebull, 1970; Fryxell, 1988), 8,000 feet in the northern Grant Range (Moores et al., 1968), and 8,000-9,000 feet in this region of eastern Nevada (Stewart, 1980).

unit name	unit abbreviation	thickness on A-A' (ft)	thickness on B-B' (ft)	published thickness (ft)	thickness shown (ft)
Windous Butte Formation	Twb	≥1700	-	-	1700 (minimum)
upper andesite flow	Tau	0-≥550	-	-	0-550 (minimum)
Stone Cabin Formation	Tsc	350-1200	≥900	-	350-1200
lower andesite flow	Tal	0-500	-	-	0-500
Sheep Pass Formation	Tsp	300-700	400	-	300-700
Ely Limestone	IPe	≥400	≥350	850-1600 (*1*)	400 (minimum)
Chainman Shale	Mc	≥700	≥350	650-2000 (*1, 3*)	1250
Joana Limestone	Mj	750	≥550	-	750
Guilmette Formation	Dg	≥1200	≥1300	1800-2200 (*1, 3*)	1800
Simonson Dolomite	Dsi	≥350	≥800	700-1000 (*1, 3*)	850 (minimum)
Oxyoke Canyon Sandstone	Doc	75	75	-	75
Sevy Dolomite	Dse	≥325	450-600	-	450-600
Laketown Dolomite	Sl	≥300	≥600	1200-1350 (*1, 2*)	1250
Ely Springs Dolomite	Oes	-	-	420 (*1*)	420
Eureka Quartzite	Oe	-	-	195 (*5*)	195
Lehman Formation	Opl	-	-	450 (*5*)	450
Kanosh Shale	Opk	-	-	150 (*5*)	150
Shingle Limestone	Ops	-	≥1150	1000 (*5*)	1150 (minimum)
Parker Spring Formation	Opp	≥600	≥800	≥1165 (*5*)	850 (minimum)
Goodwin Formation	Copg	≥2000	≥1100	≥1300 (*5*)	2050 (minimum)
Little Meadows Formation	Clm	≥300	≥300	-	300 (minimum)
Sidehill Spring Fm., Blue Eagle member	Csb	≥250	≥300	-	350 (minimum)
Sidehill Spring Fm., upper Grant Canyon member	Csgu	-	≥4050	-	4050 (minimum)
Sidehill Spring Fm., lower Grant Canyon member	Csgl	-	≥2950	-	2950 (minimum)
Sidehill Spring Fm., Willow Springs member	Csw	≥2000	≥100	-	2050 (minimum)
Pole Canyon Limestone	Cpc	≥500	-	1400 (*4*)	1400
Pioche Shale	Cp	-	-	400-800 (*2, 3, 4*)	600
Prospect Mountain Quartzite	Cpm	-	-	≥3000-4500 (*3, 4*)	4500

Data sources:
1 - Moores et al. (1968); *2* - Cebull (1970); *3* - Hyde and Huttrer (1970); *4* - Fryxell (1988); *5* - Camilleri (2013)

Table S1. Data supporting thicknesses of Grant Range rock units.

Text S2. Data supporting $^{40}Ar/^{39}Ar$ biotite age for dacite dike sample GR63.

A biotite concentrate was separated from dacite dike sample GR63 (Fig. 4; location: 38.44914° N, 115.46536° W) using standard crushing, pulverizing, and picking techniques. Thin section examination and analytical data discussed below indicate that the biotite is intergrown with hornblende and that the concentrate is a mix of the two minerals. $^{40}Ar/^{39}Ar$ analysis was performed on this sample at the New Mexico Geochronology Research Laboratory (see McIntosh et al. (2003) for discussion of methodology). In 9 heating steps, the sample did not yield a plateau (Fig. S1). Instead, steps B, C, D, and I yielded similar ages of ~29 Ma, which correspond to K/Ca ratios between 1.5 and 4, and steps E, F, G, and H yielded a range of older

ages between ~30-35 Ma, which correspond to lower K/Ca ratios between 0.7 and 1 (Fig. S1). The sample yielded an integrated age of 28.39 ± 0.02 Ma (Table S2), which, because the young age of step A balances the older ages of steps E, F, G, and H, is fortuitously similar to the ~29 Ma ages of steps B, C, D, and I. An isochron age of 31.4 ± 0.7 Ma from all 9 steps is dominated by the older steps (Fig. S2). These two ages are interpreted to represent mixing of distinct older and younger components, and are therefore not interpreted as significant.

Instead, the ~29 Ma age indicated by steps B, C, D, and I is interpreted as the approximate timing of cooling through biotite closure, and the ~30-35 Ma ages defined by steps E-H are interpreted as mixing with an apparently older, lower K/Ca component, probably hornblende. This interpretation is based on: 1) the higher K/Ca ratios (1.5-4) of steps B, C, D, and I, which are closer to those of typical biotite (K/Ca ≥10; e.g., Baxter et al., 2002), and the lower K/Ca ratios (0.7-1) of steps E-H, which are closer to those typical of hornblende (K/Ca ~0.1; e.g., Baxter et al., 2002); 2) observations of complex, multi-domain biotite crystals in thin-section, portions of which have been altered to hornblende; and 3) the position of degassing of steps E-H, which are characteristic of hornblende. During step heating, biotite generally degases over a wide temperature range between 700 and 1400°C, whereas hornblende degases over a much narrower range around 1000-1100°C (McIntosh et al., 2003). An apparent "true" age of hornblende, whether it contains excess Ar, and the geologic significance of a hornblende age are unknown.

The portion of the dacite dike that was sampled is intruded into the Cambrian Pole Canyon Limestone (unit Cpc), which restores to a pre-extensional depth of ~8 km (Figs. 3, 5). However, the sampled dike cuts faults 2 and 3 (Figs. 4, 9), and therefore, dike emplacement, at a minimum, had to post-date tectonic exhumation accommodated by motion on these two faults. Based on offset estimates on Figure 5, faults 2 and 3 collectively omit the full thickness of units Csw, Csgl, Csgu, and Clm at the sampled locality, which have a cumulative thickness of ~3 km. Therefore, the maximum permissible depth that the sampled level of the dike was emplaced at was ~5 km. Assuming a typical geothermal gradient of 30˚C/km, this maximum emplacement depth would fall well below the ~280-350˚C $^{40}Ar/^{39}Ar$ closure temperature range for biotite (Harrison et al., 1985). Therefore, the ~29 Ma age of cooling through biotite closure is interpreted as the approximate crystallization age of the dike.

ID	Power (Watts)	$^{40}Ar/^{39}Ar$	$^{37}Ar/^{39}Ar$	$^{36}Ar/^{39}Ar$ (x 10^{-3})	$^{39}Ar_K$ (x 10^{-15} mol)	K/Ca	Cl/K	$^{40}Ar^*$ (%)	^{39}Ar (%)	Age (Ma)	±1σ (Ma)
GR-63, biotite, J=0.0018789±0.02%, D=1±0, NM-268D, Lab#=62996-01											
A	1	9.741	0.1634	8.229	4.83	3.1	0.002	75.2	25.5	24.992	0.021
B	2	9.362	0.1701	3.336	4.63	3.0	0.002	89.6	50.0	28.610	0.013
C	2	9.328	0.2653	2.821	2.41	1.9	0.002	91.3	62.7	29.036	0.019
D	2	9.291	0.3207	2.525	1.89	1.6	0.002	92.2	72.7	29.226	0.022
E	2	9.774	0.5253	2.636	1.20	0.97	0.002	92.5	79.0	30.809	0.033
F	3	9.848	0.5970	2.529	0.627	0.85	0.002	92.9	82.3	31.188	0.055
G	3	11.16	0.7656	3.086	0.832	0.67	0.003	92.4	86.7	35.129	0.050
H	5	9.384	0.5287	2.578	0.623	0.97	0.002	92.3	90.0	29.547	0.055
I	21	9.211	0.3580	2.482	1.89	1.4	0.002	92.3	100.0	29.009	0.023
Integrated age ± 2σ			n=9	MSWD=6884.45	18.9	1.8				**28.386**	**0.019**
Plateau ± 2σ		no plateau	n=0	MSWD=0.00	0.000	0.000±0.000			0.0	**0.00**	**0.000**
Isochron±2σ		steps A-I	n=9	MSWD=5249.18		$^{40}Ar/^{36}Ar$=	70 ± 20			**31.402**	**0.022**

Notes:
Isotopic ratios corrected for blank, radioactive decay, and mass discrimination, not corrected for interfering reactions.
Errors quoted for individual analyses include analytical error only, without interfering reaction or J uncertainties.
Integrated age calculated by summing isotopic measurements of all steps.
Integrated age error calculated by quadratically combining errors of isotopic measurements of all steps.
Plateau age is inverse-variance-weighted mean of selected steps.
Plateau age error is inverse-variance-weighted mean error (Taylor, 1982) times root MSWD where MSWD>1.
Plateau error is weighted error of Taylor (1982).
Decay constants and isotopic abundances after Steiger and Jäger (1977).
symbol preceding sample ID denotes analyses excluded from plateau age calculations.
Ages calculated relative to FC-2 Fish Canyon Tuff sanidine interlaboratory standard at 28.201 Ma
Decay Constant (LambdaK (total)) = 5.463e-10/a
Correction factors:
$(^{39}Ar/^{37}Ar)_{Ca}$ = 0.00069 ± 0.000002
$(^{36}Ar/^{37}Ar)_{Ca}$ = 0.0002724 ± 0.0000002
$(^{38}Ar/^{39}Ar)_K$ = 0.01077
$(^{40}Ar/^{39}Ar)_K$ = 0.0072 ± 2e-05

Table S2. $^{40}Ar/^{39}Ar$ analytical data for sample GR63.

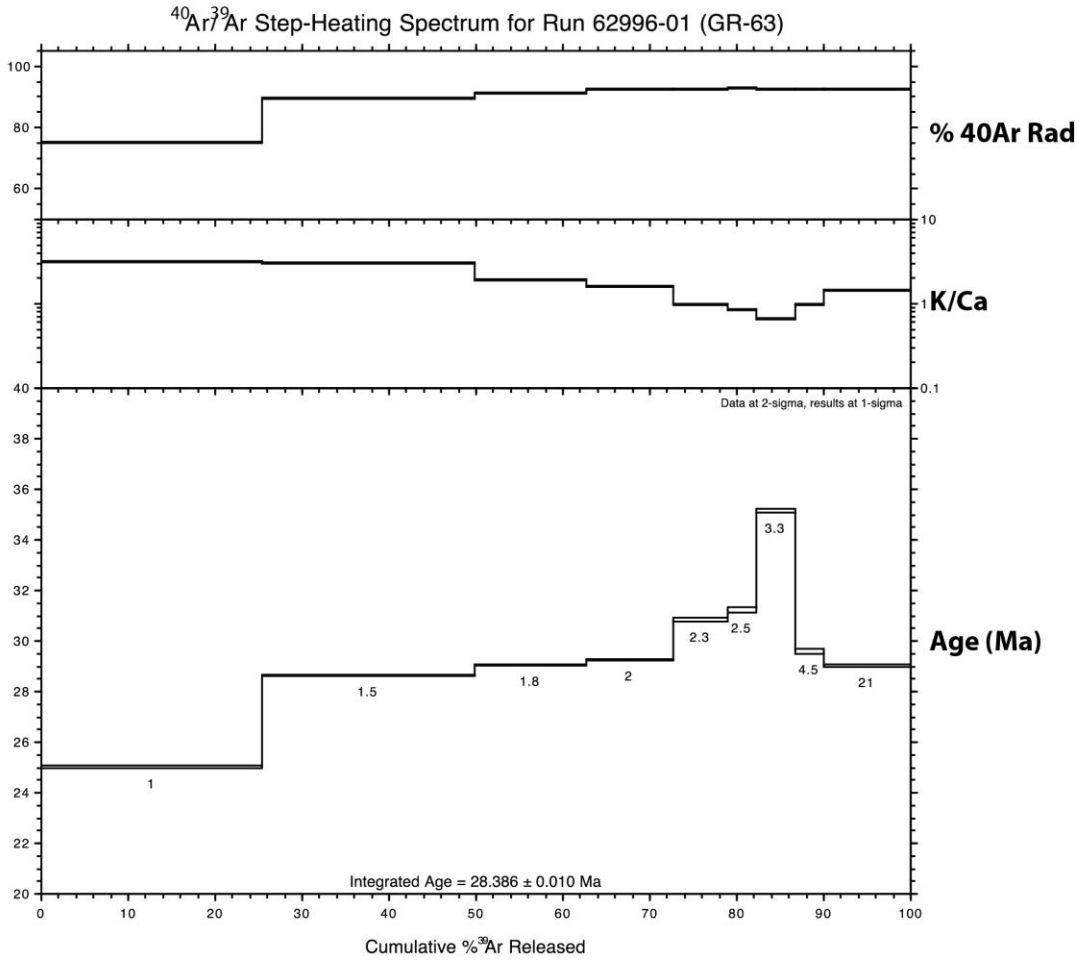

Figure S1. $^{40}Ar/^{39}Ar$ step-heating age spectra plots for sample GR63.

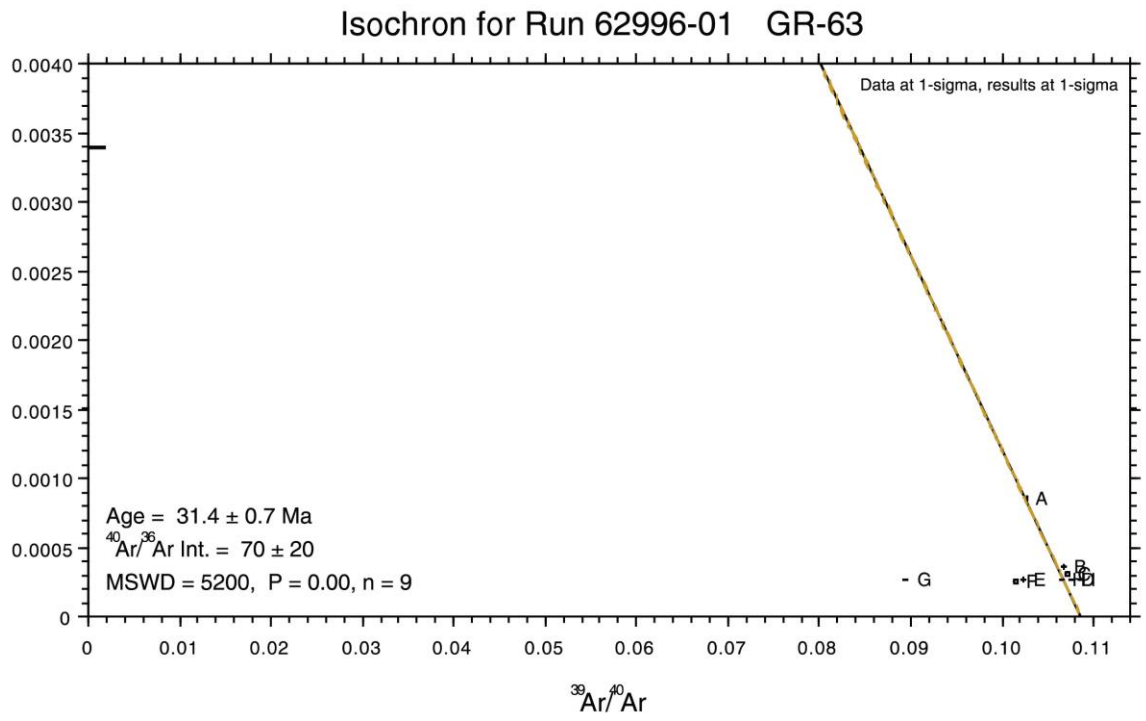

Figure S2. Inverse isochron plot for sample GR63.

Text S3. Supporting data for wells in the Grant Canyon and Bacon Flat oil fields.

Data for ten oil wells, which are distributed along an approximately east-west transect through the Grant Canyon and Bacon Flat oil fields (Fig. 2), are projected onto cross section A-A' (Fig. 5). Lithologic logs showing intersection depths of the upper contacts of rock units (formation tops), as interpreted by the original well site geologists, are compiled in Hess et al. (2004), and individual lithologic and geophysical well logs are publicly available at the Great Basin Science Sample and Records library in Reno, NV. In addition, interpretations of many of these wells are published on cross sections in several studies (McCutcheon and Zogg, 1994; Johnson, 1996; French, 1998). Formation top interpretations used in this study are summarized in Table S3.

Apparent dip data for Neogene valley fill sediment were available for nine of the wells, and apparent dip data for Paleogene and Paleozoic rocks were available for three of the wells (Fig. 5). Sources for this dip data include the cross section of McCutcheon and Zogg (1994) and the public well records at the Great Basin Science and Sample Library. Data sources for apparent dip data on specific wells are summarized on Table S3.

well abbreviation	well name	elevation (ft)	total depth (ft)	formation tops (ft)	formation tops data sources	dip data sources
BF2	Bacon Flat Federal No. 2	4707	6905	0 Tu; 1625 Qb; 1870 Tu; 5780 Tvu; 6325 IPe; 6590 Mc	5	4
BF1	Bacon Flat No. 1	4726	5450	0 Tu; 1770 Qb; 1820 Tu; 5315 Dg	2, 6	2, 4
BF24-17	Bacon Flat Federal No. 24-17	4722	5435	0 Tu; 1691 Qb; 1838 Tu; 5355 Dg	1, 2	4
GC6	Grant Canyon No. 6	4728	6260	0 Tu; 1621 Qb; 1730 Tu; 5056 Tvu; 5611 IPe; 6020 Mc; 6170 Dg	1, 2	2, 4
GC5	Grant Canyon No. 5	4718	4804	0 Tu; 4458 Dg	3, 6	no data
GC7	Grant Canyon No. 7	4731	5405	0 Tu; 3700 Dg; 4760 IPe; 5164 Mc; 5283 Mj	1	2
GC10	Grant Canyon No. 10	4730	6150	0 Tu; 3693 Dg; 4427 IPe; 4875 Mc; 5160 Mj; 5825 Dg	6	4
GC4	Grant Canyon No. 4	4737	4220	0 Tu; 4020 Dg	6	2
GC2	Grant Canyon No. 2	4740	6389	0 Tu; 4764 Dg; 5226 Mj; 5515 Dg; 6353 JKg	1, 6	2
TH1	Thorn No. 1	4809	5584	0 Tu; 5347 JKg	6	2

Data sources:

[1] this study; formation tops interpreted by J. Walker from public well records at Great Basin Science Sample and Records Library, Reno, NV

[2] McCutcheon and Zogg (1994)

[3] Johnson (1996)

[4] dip data from public well records at Great Basin Science Sample and Records Library, Reno, NV

[5] French (1998)

[6] Hess et al. (2004)

Table S3. Lithologic logs and dip data sources for wells in the Bacon Flat and Grant Canyon oil fields.

Text S4. Data constraining the geometry of set 1 faults.

Three-point problems were completed for determination of the dip angles of set 1 detachment faults (Table S4). The 'strike azimuth' was determined by locating two points of equal elevation (corresponding to the 'high elevation' column) along a fault trace. The 'low elevation' column represents a lower-elevation point measured along the fault trace, which was typically located at the bottom of a drainage. The 'elevation difference' column represents the vertical distance between the high and low elevations. The 'horizontal distance' column represents the map distance and direction (east or west is specified) measured perpendicular from the strike line that connects the two high-elevation points to the low-elevation point. The 'fault dip angle' was calculated by the equation: dip angle = $\tan^{-1}$(elevation difference/horizontal distance).

fault number	approximate UTM location (zone 11N)	strike azimuth	high elevation	low elevation	elevation difference	horizontal distance	fault dip angle
9, cross section A-A'	4258000 N, 640000 E	007°	7200'	7080'	120'	2000' E	3° E
7, cross section A-A'	4258000 N, 638500 E	358°	8400'	7200'	1200'	5000' E	13° E
6, cross section A-A'	4257200 N, 638000 E	334°	7880'	6940'	940'	7600' E	7° E
5, cross section A-A'	4257000 N, 636000 E	347°	7280'	7040'	240'	1700' E	8° E
5, northernmost part of map	4259000 N, 632600 E	348°	6800'	6000'	800'	3950' W	11° W
5, cross section B-B'	4255300 N, 636800 E	349°	7360'	6520'	840'	2950 ' E	16° E
4, used on both cross sections	4256200 N, 636000 E	355°	7200'	6340'	860'	20000' E	23° E
3, used on both cross sections	4256300 N, 635000 E	003°	6760'	6160'	600'	2800' E	17° E
2, cross section A-A'	4256500 N, 634500 E	003°	6400'	6080'	320'	850' E	21° E
2, west of culmination axis	4255000 N, 633000 E	355°	6720'	6480'	260'	2050' W	7° W

Table S4. Data supporting three-point problems for determination of Grant Range detachment fault dip angles.

Cross section A-A':	
fault number:	**geometric constraint:**
14, between wells TH1 and GC6	Dips 14° E, based on relative thicknesses of lPe and Tvu in wells GC10, GC7, and GC6, combined with subhorizontal dips of Tvu, lPe, and Mc in wells GC6 and BF2.
14, west of well GC6	Dips 0°W, based on relative thicknesses of Tvu in wells GC6 and BF2, combined with subhorizontal dips of Tvu, lPe, and Mc in wells GC6 and BF2.
13, west of well GC10	Dips 2°W, based on relative thicknesses of lPe and Mc in wells GC10, GC7, GC6, and BF2, combined with subhorizontal dips of Tvu, lPe, and Mc in wells GC6 and BF2.
12, west of well TH1	Must dip ≥20° W based on intersection depths of Jurassic-Cretaceous granite in wells TH1 and GC2. Shown at 20° W dip to maximize offset on range-bounding fault.
12, west of well TH1	Must dip ≤25° W based on projected depth of intersection of fault 10 with range-bounding fault. Shown at 20° W dip to maximize offset on range-bounding fault.
11, west of trace	Must dip ≥14° W or will intersect modern erosion surface to west, in footwall of westernmost down-to-east Neogene high-angle normal fault. Shown at 14° W dip, subparallel to fault 10.
10, east of Dg klippe	Must dip ≥8° W or will intersect modern erosion surface to east; geometry shown minimizes length of sheets 2-7 above erosion surface and therefore minimizes extension.
10, Dg klippe to trace	Dg klippe projects to 1200' above modern erosion surface; constrains dip to 12° W between klippe and trace.
10, west of trace	Must dip ≥12° W or will intersect modern erosion surface to west; must dip ≤17° W based on intersection depth of Jurassic-Cretaceous granite in well TH1; shown at 14° W dip.
8, eastern trace	Must dip ≥15° E or will intersect modern erosion surface to west; limits maximum cutoff angle to 18° with respect to Tertiary rocks and 15° with respect to Paleozoic rocks.
8, middle trace	Must dip ≥14° E or will intersect modern erosion surface to west; limits maximum cutoff angle to 19° with respect to Tertiary rocks and 16° with respect to Paleozoic rocks.
8, western trace	Must dip ≥16° E or will intersect modern erosion surface to west; limits maximum cutoff angle to 17° with respect to Tertiary rocks and 14° with respect to Paleozoic rocks.
8, all three traces	Shown at 25° E dip, in order to connect all three traces in cross section; corresponds to cutoff angle of 8° with respect to Tertiary rocks and 5° with respect to Paleozoic rocks.
1, in subsurface on west end	Footwall cutoff angle of 8° places unit Cpc at well TH1 (Fig. 5, footnote 1). Fault shown with dip angle that decreases from 30-0° toward west, so trace intersects fault 12 east of well TH1.
Cross section B-B':	
fault number:	**geometric constraint:**
10, east of Dg klippe	Must dip ≥33° W or will intersect modern erosion surface in hanging wall of high-angle set 2 normal fault to east, based on exposed thicknesses of COpg, Slm, and Dse.
10, Dg klippe to eastern trace	Must dip ≥12° W or will intersect modern erosion surface between klippe and eastern trace. Shown at 13°W dip, which connects klippe and eastern trace.
10, west end, all three traces	Three intersections of the fault trace with the modern erosion surface define a 5° W dip.
8, east end of cross-section	Must dip ≥15° E or will intersect modern erosion surface to west; limits maximum cutoff angle to 11° with respect to Tertiary and Paleozoic rocks.
8, east end of cross-section	Shown at 19° E dip, which is minimum possible dip without intersecting modern erosion surface to west, assuming constant cutoff angles across kink axes.
6, east end of cross-section	Must dip ≥7° E or will intersect modern erosion surface to east; limits maximum cutoff angle to 19° with respect to Tertiary and Paleozoic rocks on east end of cross section.
6, east of eastern trace	Shown at 0°E dip, which is minimum possible dip without intersecting modern erosion surface to east, assuming constant cutoff angles across kink axes.
6, between all three traces	Three intersections of the fault trace with modern erosion surface define a 2° W dip.
6, west of western trace	Must dip ≤3° W or will intersect modern erosion surface to west; shown at constant cutoff angle of 2° above modern erosion surface.
5, between eastern 3 traces	Intersections of the fault trace with the modern erosion surface define 5°W and 7° W-dipping segments.
5, between western 2 traces	Intersections of the fault trace with the modern erosion surface constrain a 7° W-dipping segment.
5, west of westernmost trace	Must dip ≤13°W, or will intersect modern erosion surface to west.
4, west of trace	Must dip ≥1° E or will intersect modern erosion surface to west.
3, east flank culmination window	Must dip ≥3° E or will intersect modern erosion surface to west.
3, west flank culmination window	Must dip ≤3° W because it is cut out by fault 5 to the west.
2, east flank culmination window	Must dip ≥5° E or will intersect modern erosion surface to west.
2, west flank culmination window	Must dip ≥5° W or will intersect modern erosion surface to east.
2, further west in subsurface	Must dip ≥35° W to attain observed surface thickness of COpg in footwall of set 2 normal fault; west of synclinal kink axis within COpg fault must dip ≥21° E to get trace back to surface.
1, in subsurface on west end	Constant hanging wall cutoff angle with respect to Csgl and Csgu must be ≥22° or trace will intersect modern erosion surface on west end of map area; results in variable modern dip angle.
1, in subsurface on west end	Footwall cutoff angle shown at 10° so unit Cpm is in footwall at west end of cross section, based on exposure of Cpm ca. 2 km to south of map area (Fryxell, 1988).

Table S5. Geometric constraints on Grant Range detachment faults from the cross sections.

Text S5. Data supporting retro-deformation of tilting accommodated by set 2 normal faults.

The magnitude of tilting accommodated by motion on set 2 normal faults was estimated on each cross section, by calculating the cumulative offset magnitude (Table S6). In this simple reconstruction, westward tilting accommodated by down-to-east faults was considered to have directly counteracted eastward tilting accommodated by down-to-west faults. Therefore, the total down-to-east offset was subtracted from the total down-to-west offset to generate the cumulative estimates (Table S6).

For cross-section A-A', large-offset (ca. 100-1000 m range), down-to-west faults dominate in Railroad Valley and in the eastern half of the Grant Range, with a few small-offset (ca. 30-100 m range), down-to-east faults present in the westernmost part of the Grant Range (Figs. 4, 5). Across the full width of the cross section, the cumulative offset of set 2 faults is 3.23 km of down-to-west motion (Table S6). If the range and valley are considered to represent one coherent block with a present-day width of 23.6 km, which pivoted from its western end, the magnitude of eastward tilting can be estimated either by solving trigonometrically, assuming an average fault orientation of 60°W, or by solving for the geometry of a circle with a radius of 23.6 km and a radial rotation of 3.23 km (Fig. S3). For cross section A-A', both techniques yield similar results of ~7-8° of eastward rotation (Fig. S3). This simple geometric solution assumes that tilt magnitude was homogeneous across the length of A-A', and that tilting accommodated by normal faults to the east and west of the cross section is negligible, and should therefore be considered approximate.

On cross section B-B', which stops on its western end at the trace of the down-to-west Quaternary fault that bounds the Grant Range, only two down-to-east faults of set 2 are present. However, because A-A' and B-B' are only separated by a north-south distance of ~2.5 km, it is assumed that the eastward tilt magnitude in Railroad Valley observed on A-A' is similar to the west of B-B'. Therefore, the 1.49 km of cumulative down-to-west offset (Table S6) and the 6.0 km east-west distance from the range bounding fault to point A, are projected onto B-B' (Fig. S3). This results in a cumulative offset of 820 m of down-to-west motion, and a cumulative modern length of 24.9 km. Both geometric solutions yield ~2° of eastward tilting (Fig. S3).

The ~2-8° magnitudes of eastward rotation estimated for the cross sections are corroborated by apparent dip data within Neogene valley fill sediment in the majority of oil wells projected onto A-A' (Fig. 5). Of the nine wells that have apparent dip data, seven (BF2, BF1, BF24-17, GC6, GC7, GC10, GC4) are characterized by ~5-10° eastward dips through the bottom half of the Neogene valley fill section, as the contact with Paleozoic bedrock is approached (Fig. 5). This is best illustrated at depths below ~750 m elevation on these wells. Four of these wells (BF1, GC6, GC7, GC10) show a characteristic shallowing of dips at higher stratigraphic levels in the Neogene valley fill section, which is characteristic of syn-extensional sedimentary infilling in half-grabens (e.g., Leeder and Gawthorpe, 1987). In addition, a sub-horizontal basalt flow of likely Pliocene age (Johnson, 1993; Hulen et al., 1994) within the Neogene valley fill section is intercepted at ~950 m elevation in the four westernmost wells, which also corroborates the shallowing of dips observed vertically through the Neogene valley fill section. Closer to the range front, wells GC2 and TH1 exhibit dips up to ~20-30° in Neogene valley fill, possibly indicating local rollover associated with motion on the range-bounding fault or another subsurface normal fault.

Cross section A-A':

Railroad Valley, west to east:			
location	**fault offset (m)**	**fault offset sense**	**approximate dip angle**
Bacon Flat oil field	455	down-to-west	70˚ W
Bacon Flat oil field	335	down-to-east	60˚ E
Grant Canyon oil field	305	down-to-west	60˚ W
Grant Canyon oil field	90	down-to-west	60˚ W
Grant Canyon oil field	90	down-to-west	60˚ W
range-bounding fault	885	down-to-west	60˚ W
cumulative:	**1490**	**down-to-west**	
Grant Range, west to east:			
location	**fault offset (m)**	**fault offset sense**	**approximate dip angle**
West Heath Canyon	90	down-to-east	60˚ E
West Heath Canyon	90	down-to-east	60˚ E
West Heath Canyon	30	down-to-east	60˚ E
West Heath Canyon	90	down-to-east	60˚ E
West Heath Canyon	120	down-to-east	60˚ E
West Heath Canyon	60	down-to-west	60˚ W
Eastern half of range	120	down-to-west	65˚ W
Eastern half of range	60	down-to-east	62˚ E
Eastern half of range	975	down-to-west	60˚ W
Eastern half of range	915	down-to-west	47˚ W
Eastern half of range	150	down-to-west	60˚ W
cumulative:	**1740**	**down-to-west**	
Grant Range and Railroad Valley cumulative offset	**3230**	**down-to-west**	

Cross section B-B':

location	**fault offset (m)**	**fault offset sense**	**approximate dip angle**
western fault	60	down-to-east	60˚ E
eastern fault	610	down-to-east	60˚ E
cumulative:	**670**	**down-to-east**	
Railroad Valley: cumulative offset projected from A-A'	**1490**	**down-to-west**	
Grant Range and Railroad Valley cumulative offset	**820**	**down-to-west**	

Table S6. Offset magnitudes of set 2 normal faults.

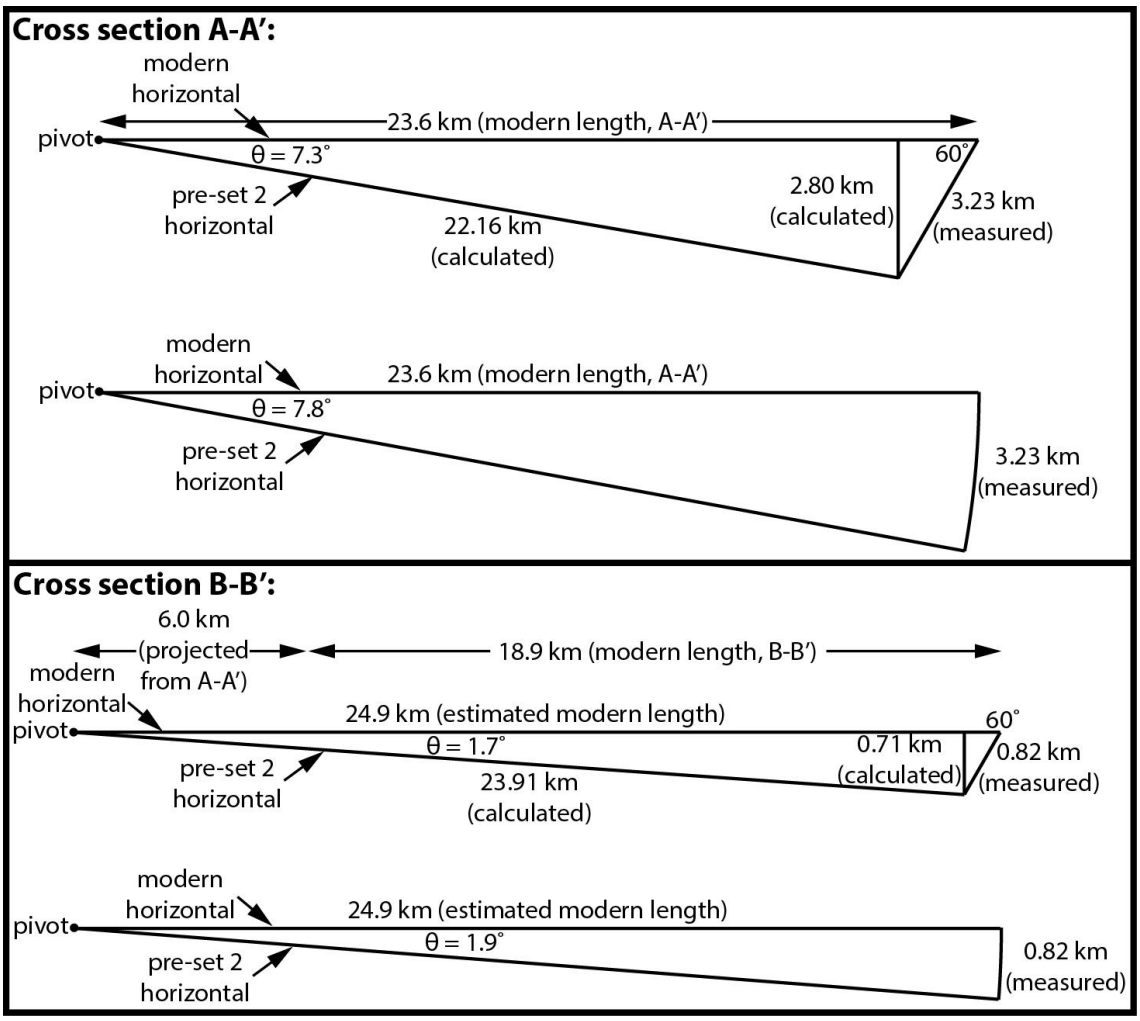

Figure S3. Simple geometric models used to estimate tilt magnitude accommodated by set 2 normal faults. For each cross section, the top model shows rotation estimated by cumulative slip along a 60˚ west-dipping normal fault, and the bottom model shows circular rotation about a pivot located at the western end of the cross-section. Diagrams are not drawn to scale.

Text S6. Detailed descriptions of geometries and field relationships of set 1 faults.

Fault 1: Fault 1 is exposed for a map distance of ~1 km on the south side of Heath Canyon, west of the culmination axis. It is cut by fault 2, making it the oldest and structurally-lowest set 1 fault exposed in the map area. At its trace, it places unit Csgu over unit Csw, corresponding to omission of at least 800 m of stratigraphy, and offset estimates on the cross sections are 5150-5400 m. On cross section B-B', fault 1 must cut down section toward the west in its hanging wall through a minimum thickness of 2100 m of units Csgu and Csgl in order for its trace to not intersect the modern erosion surface. On the basis of exposures of unit Cpm

observed ~2 km to the south of the map area (Fryxell, 1988), fault 1 must cut down section toward the west in its footwall through units Csw, Cpc and Cp by the western edge of the map area. Exposures of unit Cpm south of the map area imply that the trace of fault 1 is at a shallow depth below the modern erosion surface on the western end of B-B'. Assuming that cutoff angles stay constant across strike, this relationship, along with thicknesses and dip magnitudes of rocks in its hanging wall on B-B', indicates a progressive westward shallowing of dip angle, which provides evidence for syn- or post-emplacement folding of fault 1 on the western flank of the culmination. On cross section B-B', fault 1 is shown flattening westward from a dip of 59˚W, through horizontal, to 13˚E, corresponding to a ~70˚ change in dip angle on the western flank of the culmination. Because this geometry is based on assumption of constant cutoff angles across-strike, the amount of syn-extensional folding that this relationship implies should be interpreted as a maximum.

On cross section A-A', granite intercepted in wells TH1 and GC2 is interpreted as part of the Jurassic-Cretaceous Troy stock, which intrudes rock units no shallower than Cpc to the south of the map area (Fryxell, 1988). Based on interception of Cambrian marble in nearby well Heath Canyon No. 15-14 (Hess et al., 2004), unit Cpc is interpreted as the most likely stratigraphic level of granite intrusion in wells TH1 and GC2. Therefore, fault 1 is shown shallowing in dip toward the west, so that well TH1 intercepts granite intruded into unit Cpc in its footwall; this implies folding of fault 1 on the western flank of the culmination, similar to cross-section B-B'.

Fault 2: In Heath Canyon, fault 2 places units Clm and Csb over units Cpc and Csw in the autochthon, corresponding to omission of 2100-3100 m of stratigraphy. On the south side of Heath Canyon, west of the trace of fault 1, fault 2 places Csb over Csgu, corresponding to omission of 100-1000 m of stratigraphy. Offset on fault 2, estimated using unit thicknesses and subsurface projection of the cutoff angles measured in Heath Canyon, is ca. 13-15 km. Fault 2 cuts fault 1, and is cut by fault 3. In addition, fault 2 is cut by an undated, E-trending granite dike (unit Tgd) on the south side of Heath Canyon, and is cut by a NE-trending, ~29 Ma (sample GR63) dacite dike (unit Tdd) on the north side of Heath Canyon. Fault 2 also displays evidence for syn- or post-emplacement folding across the culmination axis. In Heath Canyon, fault 2 dips 17-21˚E on the east side of the culmination axis. On cross-section B-B', where the autochthon is exposed in a window below fault 2, the dip of fault 2 is 5˚E on the eastern flank of the window and 5˚W on the western flank of the window. To the west, a minimum subsurface dip of 35˚W is required to maintain the observed stratigraphic thicknesses of rocks in the hanging wall of fault 2. From west to east, these data collectively record ~50˚ of difference in dip angle over the culmination, corresponding to folding of the trace of fault 2 into an anticline with an interlimb angle of ~130˚.

Fault 3: Fault 3 dips 17˚E in Heath Canyon, and places unit COpg over unit Clm. Offset and stratigraphic omission estimates of 50 m and 10 m, respectively, are approximated for fault 3; however, because only minimum tectonic thicknesses are available for units COpg and Clm, these estimates should be interpreted as minima. Fault 3 cuts fault 2 on the north side of Heath Canyon, and fault 2 is the youngest fault to be cut by the NE-trending, ~29 Ma dacite dike (unit Tdd) on the north side of Heath Canyon.

Fault 4: Fault 4 dips 23˚E in Heath Canyon, where it places unit Opp over unit COpg. Similar to fault 3, as only minimum tectonic thicknesses are available for units COpg and Opp, offset

estimates of 600 m on A-A′ and 50 m on B-B′, and stratigraphic omission estimates of ~250 m on A-A′ and ~10 m on B-B′ should be interpreted as minima. Fault 4 is cut by fault 5 on the north and south sides of Heath Canyon.

Fault 5: Fault 5 typically places unit Slm, and locally units Dse, Doc, and Dsi, over Cambrian and Ordovician units ranging from Cpc to Ops. Fault 5 consistently cuts down section in its footwall toward the west, and omits progressively more section as it cuts older faults toward the west. Stratigraphic omission across fault 5 ranges from 300-1400 m at its eastern trace in Heath Canyon (including omission of units Opk, Opl, Oe, and Oes, which are not exposed in the map area but are observed ~3 km to the north on the map of Camilleri (2013)), to a cumulative omission of 4300-5000 m at its northwestern exposure, where it places Slm over Csw. Offset is estimated at 2500 m on cross section A-A′, which is a minimum estimate based on offset of a kink axis that is projected above and below the erosion surface. On cross section B-B′, fault 5 exhibits multiple across-strike exposures, indicating greater across-strike structural overlap, and offset is estimated at 8850 m. On cross section B-B′, fault 5 exhibits sections that cut both gently upsection and downsection across strike in its hanging wall, at cutoff angles ≤15˚, indicating ~300 m of structural relief on the fault plane. At the northern end of the map, west of the culmination axis, fault 5 cuts faults 2 and 3. On the north side of Heath Canyon, at the culmination axis, fault 5 cuts fault 4, and is cut by fault 10. On the south side of Heath Canyon, fault 5 cuts faults 2, 3, and 4, and cuts the undated, east-trending granite dike (unit Tgd) that cuts fault 2.

Fault 5 exhibits evidence for syn- or post-emplacement folding over the culmination axis, which is visible in its map pattern, and is illustrated on the cross sections. On cross section B-B′, the dip of fault 5 changes from 16˚E east of its easternmost trace, to 5-7˚W between the four traces that intersect the cross section line, to 13˚W west of its westernmost trace. This defines a ~30˚ change in dip angle across the culmination axis, corresponding to folding of the trace of fault 5 into an anticline with an interlimb angle of ~150˚. On cross section A-A′, east of the culmination axis, fault 5 dips 8˚E on the north side of Heath Canyon. North of the cross section line, the trace of fault 5 approaches horizontal at the culmination axis, where it is cut by fault 10. West of the culmination axis, at the northern end of the map area, fault 5 dips 11˚W. These data indicate a ~20˚ change in dip across the culmination axis, corresponding to folding of the trace of fault 5 into an anticline with an interlimb angle of ~160˚.

In addition, on the south side of Heath Canyon, at the culmination axis, fault 5 incises through sheet 2 for an across-strike distance of ~300 m, placing sheet 5 directly over the autochthon, while sheet 2 is observed under fault 5 to the east and west. This relationship, combined with the greater interlimb angle of structurally-higher, younger fault 5 compared to fault 2, argues for positive gain in structural elevation of the culmination axis with progressive extension.

Fault 6: Fault 6 places unit Dg over unit Dsi across the full N-S width of the map area, and exhibits dip angles between 0-7˚E and cutoff angles between 2-7˚. Above the erosion surface on cross section B-B′, based on continuous across strike exposure of sheet 5, fault 6 must maintain a shallow footwall cutoff angle in order to not intersect the modern erosion surface west of culmination axis. Stratigraphic omission and offset on fault 6 depend on published thicknesses of units Dsi and Dg (Moores et al., 1968; Hyde and Huttrer, 1970), and are estimated at 150-300 m and 1300-4300 m, respectively. Fault 6 is cut by fault 7 on the south side of Heath Canyon.

Fault 7: Fault 7 places Mj over Dg, except in one locality on the south side of Heath Canyon where fault 7 cuts fault 6 and places Mj directly over Dsi. Fault 7 dips 13˚E on the north side of Heath Canyon, which results in hanging wall and footwall cutoff angles of -2˚ on cross section A-A'. On the east end of cross section A-A', fault 7 is interpreted at a shallow depth in the subsurface, based on exposure of fault 7 in the footwall of a set 2 normal fault ~500 m to the south of the cross section line. Subsurface correlation of this trace with the westernmost trace, on the basis of relative thicknesses of units Mj and Dg in its footwall and hanging wall, indicates that fault 7 has segments that cut gently downsection and upsection in the transport direction, corresponding to ~300 m of across strike structural relief on the fault plane (Fig. 10). Stratigraphic omission on fault 7 is estimated at a maximum of 150 m, and offset is estimated at 4800 m. This offset estimate depends on a poorly-constrained subsurface geometry, and should be considered approximate. Fault 7 is not observed on cross-section B-B', indicating that it either merges with, or is cut out by, fault 8 above the modern erosion surface between the A-A' and B-B' section lines.

Fault 8: Fault 8 places Mc over Mj, except in one locality on the north side of Heath Canyon where fault 8 cuts fault 7 and places Mc directly over Dg. On A-A', connecting the three intersected across strike traces in the subsurface yields a 25˚E dip, which defines 8˚ and 5˚ cutoff angles with respect to Tertiary and Paleozoic rocks, respectively. In the northeast corner of the map, the dip angle of fault 8 requires that it cuts Tsp in the subsurface to the east of its trace, and by inference units Tal, Tsc, and Tau as well because of similar tilt magnitudes between these units. On cross section B-B', at the east end of the range, fault 8 is shown at a minimum dip of 19˚E, which defines 6˚ cutoff angles with respect to Paleozoic and Tertiary rocks. Stratigraphic omission across fault 8 is estimated at 300 m at its eastern trace, and offset estimates range from 3100-4100 m.

Fault 9: Fault 9 places units lPe, Tsp, and Tsc over Mc. Fault 9 is observed to cut stratigraphically-higher rock units (Tsp, Tsc) than any other set 1 fault, and is inferred to cut unit Twb above the modern erosion surface (Fig. 5). Fault 9 has a modern dip angle of 3˚E, and exhibits 27-30˚ cutoff angles with respect to Paleozoic and Tertiary rocks. Fault 9 is inferred to merge with fault 8 above the modern erosion surface to the west of its trace (Fig. 5). Stratigraphic omission is estimated at 350 m, and offset is estimated at 700 m.

Fault 10: Fault 10 places units Dg and Mj over units Csw and Csgu along its main trace on the western flank of the Grant Range. Two additional structures are correlated with fault 10, a fault bounding a klippe of Dg in the southwest corner of the map area, visible on cross section B-B', which places Dg over COpg, and a fault bounding the base of an exposure of units Dg, Mj, and Mc at the culmination axis on the north side of Heath Canyon, which is deformed by several second-order faults, and includes the Dg klippe that is projected onto cross section A-A'. On cross section A-A', a modern dip angle of 12˚W is defined between the Dg klippe and the main trace of fault 10 to the west, which defines a footwall cutoff angle of -9˚ and a hanging wall cutoff angle range of -3˚ to 13˚. East of the Dg klippe, the geometry of fault 10 is unconstrained. It is shown with a dip angle of 8˚W on cross section A-A', which minimizes the length of sheets 2-7 above the erosion surface, thereby minimizing extension. This geometry defines footwall cutoff angles with sheets 2-7 that range from 18-44˚. Fault 10 cuts fault 5 near the culmination axis, which requires that it must cut faults 2-4 above the modern erosion surface on A-A'. Cross-cutting relationships between fault 10 and faults 6-9 are not observed. Fault 10 carries stratigraphically-higher rocks than fault 6, which implies that it cuts fault 6

above the erosion surface. Fault 10 carries similar stratigraphic levels to fault 7, and it is possible that faults 7 and 10 are correlative, and connect above the erosion surface, as shown in Lund et al. (1993). However, because no cross-cutting relations are exposed, because the restored position of rocks in the hanging wall of fault 10 is not constrained, and because the 7.0 km of structural overlap on fault 10 shown on A-A' is greater than the 4.8 km of offset shown on fault 7, faults 7 and 10 cannot be confidently correlated, and they are discussed here as two separate faults.

On cross-section B-B', fault 10 dips 5˚W between the three traces exposed on the western flank of the Grant Range, dips 13˚W between the eastern of these traces and the Dg klippe, and must dip at least 33˚W above the erosion surface to the east of the Dg klippe in order to not intersect the modern erosion surface in the hanging wall of a set 2 fault to the east. This defines at least ~30˚ of westward shallowing of the dip of fault 10 across the western flank of the culmination, which provides further evidence for syn- and post-emplacement folding. These dip magnitudes correspond to hanging wall cutoff angles between -7˚ and 2˚, and footwall cutoff angles of 26-48˚ with respect to sheet 1, 16˚ with respect to the autochthon, and 32-35˚ with respect to sheets 2 and 5. Fault 10 cuts fault 1, and map relations require that it cuts faults 2 and 5 above the modern erosion surface on B-B'. On the basis of projected cutoff angles between their traces, faults 10 and 8 carry similar stratigraphic levels on B-B'. However, because the restored position of sheet 10 is not constrained, and because of the great distance between the traces of faults 8 and 10, these two faults cannot be confidently correlated.

Stratigraphic omission across fault 10 ranges widely, as a result of cumulative omission of older, structurally-lower set 1 faults toward the west, and is as high as 5200 m where it places Dg over Csgl in sheet 1 at the southwest corner of the map area, and 5400 m where it places unit Mj over unit Csw in the autochthon in Heath Canyon. The restored position of sheet 10 is not constrained, so offset cannot be precisely estimated. The minimum offset of fault 10, estimated from observed across-strike structural overlap, is 4600 m on cross-section B-B', and 7000 m on cross-section A-A'.

Fault 11: On the western flank of the Grant Range, four spatially-isolated faults that place Dg over Mj, and one fault that places Dg over Mc, corresponding to duplication of 150-350 m of stratigraphy, are correlated as segments of fault 11. The southernmost segment was interpreted as a thrust fault by Lund et al. (1988), and the segment that places Dg over Mc was originally interpreted as a thrust fault by Lund et al. (1987). On cross section A-A', fault 11 is shown subparallel to fault 10, with a dip angle of 14˚W; a shallower dip angle would result in the trace intersecting the modern erosion surface to the west. Fault 11 exhibits -3˚ cutoff angles with respect to hanging wall and footwall rocks. The restored position of sheet 11 is unconstrained; offset on fault 11 is estimated at a minimum of 4000 m, based on observed structural overlap. Fault 11 cuts fault 10 in one locality on the south side of Heath Canyon.

Fault 12: Fault 12 is the designation for the structure that places unit Dg over Jurassic-Cretaceous granite (unit JKg) in well GC2. To the west of well GC2, the rocks carried by fault 12 consist of a stratigraphically-intact section of units Dg, Mj, and Mc, which are drafted to the deepest level drilled within unit Dg (Fig. 5). Fault 12 has a minimum dip of 20˚W, based on intersection depths of JKg in wells TH1 and GC2, and is shown at a 20˚W dip to maximize offset on the range-bounding fault. This defines hanging wall cutoff angles of 20˚ and 34˚ with

respect to sheets 12 and 14, respectively, and footwall cutoff angles of 28˚ with respect to the autochthon and 40˚ with respect to sheet 1. The geometry of fault 12 east of well TH1 is unconstrained; it is possible that fault 12 and fault 10 share a similar, master footwall detachment level, and this geometry is shown in cross section A-A'. However, faults 12 and 10 exhibit differing hanging wall stratigraphic levels, and lateral continuity between sheets 12 and 10 cannot be confidently demonstrated. It is possible that one or more set 1 faults splay upward off of fault 12 between well TH1 and the range front fault (e.g., Fig. 9B). On this basis, faults 12 and 10 are discussed here as separate structures. Stratigraphic omission across fault 12 at well GC2 is estimated between 5400-6200 m, which is the largest omission in the study area. The restored position of rocks carried by fault 12 is unconstrained; a conservative, minimum offset estimate of 2800 m can be made on the basis of observed structural overlap.

Fault 13: Fault 13 places unit lPe over unit Mc, and was interpreted based on ca. 50-75 m thicknesses of Mc encountered in wells GC10, GC6, and BF2. This is much thinner than the ca. 300 m minimum thickness for Mc observed in the Grant Range, and therefore a bedding-subparallel detachment fault (fault 13) is interpreted at the top of unit Mc on cross section A-A'. Fault 13 carries up to 100 m of unit lPe, intercepted in wells GC10, GC7, GC6, and BF2, which is overlain by at least 200 m of undifferentiated Paleogene volcanic rocks (unit Tvu), intercepted in wells GC6 and BF2 (Fig. 5). Subhorizontal to gently east-dipping apparent dips observed in units lPe and Tvu on wells GC6 and BF2 indicate that the Paleogene unconformity has minimal angular discordance here, similar to surface observations on the eastern end of the Grant Range. Intersections of fault 13 in multiple wells define a 2˚W dip, corresponding to 2˚ hanging wall and footwall cutoff angles. Fault 13 omits ~250 m of Mc and an unknown thickness of lPe. Restoration of offset on the basis of the observed cutoff angle would indicate ≥10,000 m of offset on fault 13; however, since the restored positions of sheets 12 and 13 are not constrained, the observed minimum structural overlap of 1600 m is used as a conservative, minimum offset estimate. The absence of unit lPe in well GC2 requires that fault 13 is cut by fault 14 on its eastern end.

Fault 14: Fault 14 is interpreted based on older-over-younger relationships of Dg overlying lPe in wells GC10 and GC7, and interceptions of Dg in wells BF24-17 and BF-1 that are at shallower depths than the intersections of units lPe and Tvu in well BF2 (Fig. 5). In addition, structurally-high intersections of unit Dg in wells GC2, GC4, and GC5 lend support to the across-strike continuity of a sheet of Dg to the east and west of its interceptions in wells GC10 and GC7 (Fig. 5). In A-A', fault 14 is shown with an apparent west-vergent thrust geometry, ramping upsection at a cutoff angle of 14˚ through units Mc, Mj, lPe, and Tvu in its footwall, with a bedding-parallel footwall flat west of well GC6. The hanging wall cutoff angle is 0˚, on the basis of the relative thickness and structural height of Dg intercepted in across-strike drill holes, and subhorizontal apparent dips within unit Dg in well BF1. West of the top of the footwall ramp, fault 14 duplicates a maximum of ca. 950 m of section. The restored position of sheet 14 is unconstrained, so offset cannot be accurately assessed. A minimum across strike structural overlap of 2600 m serves as a conservative, minimum offset estimate.

Fault 14 cuts fault 13, and cuts unit Tvu. No cross-cutting relationships between faults 14 and 12 are exposed; on the basis of their relative dip angles, fault 14 is inferred to branch westward off of fault 12. In addition, though they both repeat strata, lateral continuity between sheet 14 and sheet 11 cannot be demonstrated. On the basis of their hanging wall cutoff angles, and the relative stratigraphic levels that they carry, faults 14 and 11 are most likely not correlative.

At its westernmost exposure, fault 11 carries unit Mj in its hanging wall. However, fault 14 carries at least ~300 m of unit Dg in its hanging wall. Therefore, if these two faults are correlative, fault 11 would have to cut down section through ~350 m of stratigraphy between its westernmost exposure and well GC2. While this is possible, this would be significantly different than the hanging wall cutoff angles shown for these two faults on A-A'.

Interpretations of well data in the Grant Canyon and Bacon Flat oil fields in previous studies have yielded varying geometries and genetic interpretations for the older-over-younger relationships that are used here to define fault 14. McCutcheon and Zogg (1994) interpreted an east-vergent thrust fault that places Devonian rocks over Mississippian and Pennsylvanian rocks. Hulen et al. (1994) interpreted the sheet of Dg as the hanging wall of a Mesozoic thrust fault, with no vergence direction specified, and compared this structure to thrust faults mapped in the western Grant Range by Lund et al. (1987; 1988), which are interpreted in this study as segments of fault 11. Johnson (1993) and French (1993; 1998) interpreted the Dg sheet as a detached, Tertiary gravity-slide block that slid westward from the western flank of the Grant Range. We propose that fault 14 is part of the set 1 detachment system, with an apparent thrust-sense offset. In section 6.1 in the text, a geometric mechanism is presented that allows interpreting fault 14 in the context of the kinematic development of the set 1 fault system.

References cited in supporting information

Baxter, E.F., D.J. DePaolo, and P.R. Renne (2002), Spatially correlated anomalous $^{40}Ar/^{39}Ar$ "age" variations in biotites about a lithologic contact near Simplon Pass, Switzerland: a mechanistic explanation for excess Ar: *Geochim. Et Cosmochim. Acta*, 66, 1067-1083.

Camilleri, P.A. (2013), Geologic map and structure of the west-central part of the Grant Range, Nye County, Nevada: *Geol. Soc. Am. Dig. Map Chart Ser.*, 14, 25 p., doi: 10.1130/2013.DMCH014.

Cebull, S.E. (1970), Bedrock geology and orogenic succession in southern Grant Range, Nye County, Nevada: *Am. Assoc. Petrol. Geol. Bull,* 54, 1828-1842.

French, D. E. (1993), Debris slides of the Railroad Valley area, Nye County, Nevada: yet another interpretation of Grant Canyon and Bacon Flat fields (abs.): *Am. Assoc. Petrol. Geol. Bull.*, 77, 1448.

French, D.E. (1998), Petroleum geology of Bacon Flat and Grant Canyon fields, in *Hydrocarbon Habitat and Special Geologic Problems of the Great Basin*, edited by D.E. French and R.A. Schalla, *Nev. Petol. Soc. 1998 Field Trip Guidebook*, Reno, Nevada, 68-70.

Fryxell, J.E. (1988), Geologic map and description of stratigraphy and structure of the west-central Grant Range, Nye County, Nevada: *Geol. Soc. Am. Map Chart Ser.,* MCH064, 16 p.

Harrison T.M., I. Duncan, and I. McDougall (1985), Diffusion of ^{40}Ar in biotite: temperature, pressure and compositional effects: *Geochim Cosmochim Acta*, 49, 2461-2468

Hess, R.H., S.P. Fitch, and S.N. Warren (2004), Nevada oil and gas well database: *Nev. Bur. Mines Geol. Open-File Rep.* 04-1.

Hulen, J.B., F. Goff, J.R. Ross, L.C. Bortz, and S.R. Bereskin (1994), Geology and geothermal origin of Grant Canyon and Bacon Flat oil fields, Railroad Valley, Nevada: *Am. Assoc. Petrol. Geol. Bull.*, 78, 596-623.

Hyde, J.H., and G.W. Huttrer (1970), Geology of the central Grant Range, Nevada: *Am. Assoc. Petrol. Geol. Bull.,* 54, 503-521.

Johnson, E.H. (1993), A look at Bacon Flat, Grant Canyon oil fields of Railroad Valley, Nevada: *Oil and Gas Journ.*, 91, 64–68.

Johnson, E.H. (1996), The structure of the Grant Canyon and Bacon Flat oil fields, Nevada, as revealed by 3-D seismic data, in *Am. Assoc. Petrol. Geol. Studies in Geology No. 42* and *Soc. Econ. Geol. Geophysical Developments Series No. 5*, edited by P. Weimar and T.L. Davis, Tulsa, Oklahoma, p. 237-246.

Leeder, M.R., and R.L. Gawthorpe (1987), Sedimentary models for extensional tilt-block/half-graben basins, in *Continental Extensional Tectonics,* edited by M.P. Coward, J.F. Dewey, and P.L. Hancock, *Geol. Soc. Am. Spec. Publ. 28*, 139-152.

Lund, K., J.T. Nash, L.S. Beard, H.R. Blank, Jr., and S.E. Tuftin (1987), Mineral resources of the Blue Eagle wilderness study area, Nye County, Nevada: *USGS Bull.*, 1731-D, 19 p.

Lund, K., L.S. Beard, H.R. Blank, Jr., A.H. Hofstra, and M.M. Hamilton (1988), Mineral resources of the Riordans Well wilderness study area, Nye County, Nevada: *USGS Bull.*, 1731-H, 16 p.

Lund, K., S.L. Beard, and W.J. Perry (1993), Relation between extensional geometry of the northern Grant Range and oil occurrences in Railroad Valley, east-central Nevada, *Am. Assoc. Petrol. Geol. Bull.* 77, 945-962, doi: 10.1306/BDFF8DA8-1718-11D7-8645000102C1865D

McCutcheon, T.J., and W.D. Zogg (1994), Structural geology of the Grant Canyon-Bacon Flat field area, Nye County, Nevada: Implications for hydrocarbon exploration in the Great Basin, in *Oil Fields of the Great Basin*, edited by R.A. Schalla and E.H. Johnson, *Nev. Petrol. Soc. Spec. Publ.*, Reno, Nevada, 201-226.

McIntosh, W.C., M. Heizler, L. Peters, L., and R. Esser (2003), $^{40}Ar/^{39}Ar$ geochronology at the New Mexico Bureau of Geology and Mineral Resources: *New Mexico Bur. Geol. Min. Res. Open File Rep.* OF-AR-1, 10 p.

Moores, E.M., R.B. Scott, and W.W. Lumsden (1968), Tertiary tectonics of the White Pine-Grant Range, east-central Nevada, and some regional implications: *Geol. Soc. Am. Bull.,* 79, 1703-1726.

Steiger, R.H., and E. Jäger (1977), Subcommission on geochronology: Convention on the use of decay constants in geo- and cosmochronology: *Earth Plan. Sci. Lett.* 36, 359-362.

Taylor, J.R. (1982), *An Introduction to Error Analysis: The Study of Uncertainties in Physical Measurements*, University Science Books, Mill Valley, California, 270 p.